Changes in gill and air-breathing organ characteristics during the transition from water- to air-breathing in juvenile *Arapaima gigas*

Andrea Y. Frommel, Garfield T. Kwan, Kaelan J. Prime, Martin Tresguerres, Henrik Lauridsen, Adalberto L. Val, Ligia U. Gonçalves, Colin J. Brauner

Abstract

The obligate air-breathing Amazonian fish, *Arapaima gigas*, hatch as water-breathing larvae but with development, they modify their swim bladder to an air-breathing organ (ABO) while reducing their gill filaments to avoid oxygen loss. Here, we show that significant changes already take place between 4 weeks (1.6 g) and 11 weeks (5 g) post hatch, with a reduction in gill lamellar surface area, increase in gill diffusion distance, and proliferation of the parenchyma in the ABO. By using a variety of methods, we quantified the surface area and diffusion distances of the gills and skin, and the swim bladder volume and anatomical complexity from hatch to 11-week-old juveniles. In addition, we identified the presence of two ionocyte types in the gills and show how these change with development. Until 1.6 g, *A. gigas* possess only the H^+-excreting/Na^+-absorbing type, while 5-g fish and adults have an additional ionocyte which likely absorbs H^+ and Cl^- and excretes HCO_3^-. The ionocyte density on the gill filaments increased with age and is likely a compensatory mechanism for maintaining ion transport while reducing gill surface area. In the transition from water- to air-breathing, *A. gigas* likely employs a trimodal respiration utilizing gills, skin, and ABO and thus avoid a respiratory–ion regulatory compromise at the gills.

Highlights

- Significant transformations in gill, skin, and ABO between 1.6 and 5.5 g body mass of *A. gigas* with the transition from water- to air breathing Larval *A. gigas* gills have one ionocyte type for Na^+ and H^+ regulation, while older juveniles and adults have an additional ionocyte type for Cl^- and HCO3$^-$

1 INTRODUCTION

Arapaima gigas is one of the largest freshwater fishes in the world, inhabiting hypoxic and ion-poor waters and flooded forests of the Amazon River basin. One of the most obligate air-breathing fishes, it drowns within about 10 min if denied access to the water surface (Val & de Almeida-Val, 1995).

Like all air-breathing fishes (Graham, 1997), the larvae hatch as water-breathers, and presumably use their skin and gills to extract O_2 from the water. A week after the larvae hatch (~1 g, 1.7–1.8 cm length), the breeding male guides the larvae to the surface where they take their first gulp of air (Graham, 1997; Lüling, 1964). By the time they reach 4–6 g (2–3 weeks post hatch), over 60% of their O_2 uptake is from the air (Pelster et al., 2020). At 10 g, they drown without access to air (and thus, by definition, are obligate air-breathers), however, they can still survive up to 20 min without access to air—twice as long as a 1-kg *A. gigas* (Brauner et al., 2004). In *A. gigas* that are 0.70–2 kg, approximately 80% of their O_2 uptake occurs through aerial respiration at a ventilation rate of one breath every 1–4 min (Stevens & Holeton, 1978), with only 5%–20% of O_2 uptake occurring at the gills (Brauner & Val, 1996; Stevens & Holeton, 1978). Thus, in early life stages of *A. gigas*, the majority of the transition from gill to air-breathing organ (ABO) O_2 uptake likely occurs before 4–6 g (Pelster et al., 2020). It is worth mentioning that all these studies were conducted under normoxia and thus it is unclear how development under hypoxia may affect ontogenetic transition rates.

The transition from water- to air-breathing in fishes is associated with physiological adaptations to accomplish gas exchange, ionoregulation, acid–base balance and nitrogenous waste excretion (Brauner &

Berenbrink, 2007; Cameron & Wood, 1978; Graham, 1997; Pelster & Wood, 2018; Shartau & Brauner, 2014). The gills of a 10-g *A. gigas* possess lamellae, but these are more compact than in regular water-breathing fishes (Brauner et al., 2004; Fernandes et al., 2012). As *A. gigas* grows from 10 g to 1 kg in 4–5 months, the gill lamellae gradually atrophy filling the interlamellar space to the point that the filaments appear as smooth rods. As a result, the gill epithelium becomes thicker and its surface area is greatly reduced, which reduces gas permeability and diffusive ion loss (Brauner et al., 2004). Concurrently, the thickening of the dermis prohibits cutaneous respiration, while the ABO volume increases and becomes highly vascularized to maximize O_2 uptake into the blood (Graham, 1997). At ~100 g, the ABO is fully functional with a total surface area 2.8 times that of the gills, and a diffusion distance 1/43rd that of the gills (Fernandes et al., 2012).

The reduction in gill surface area and thickening of branchial surfaces and skin, along with the increased reliance on air-breathing, impairs CO_2 excretion. As a result, pCO_2 within the *A. gigas* blood gradually increases to about 16 mmHg at 700 g (Gonzalez et al., 2010) and >30 mmHg in 1–2 kg fish (Randall et al., 1978; Wood et al., 2020), the latter of which is ~10-fold higher than the average water-breathing fish (Brauner et al., 2019; Evans et al., 2005). However, the blood pH of adult *A. gigas* stays relatively high (~7.6; Gonzalez et al., 2010; Randall et al., 1978) and is associated with greatly elevated plasma [HCO_3^-], implying that *A. gigas* lives in a constant state of compensated respiratory acidosis compared with a water-breathing fish (Brauner et al., 2004; Shartau & Brauner, 2014) Despite their reduced branchial surface area, most of *A. gigas*'s CO_2 excretion takes place across the gills, as the ABO and kidneys combined account for only for ~10%–40% (Brauner & Val, 1996; Pelster et al., 2020; Randall et al., 1978). Although the kidney of adult *A. gigas* plays an important role in nitrogen waste excretion (Gonzalez et al., 2010; Hochachka et al., 1978; Wood et al., 2020), the urine contains nearly equal amounts of NH_4^+ and HCO_3^-, precluding a major role of kidneys in blood acid–base regulation (Wood et al., 2020). Thus, similar to water-breathing fishes, *A. gigas* blood acid–base regulation is likely achieved predominantly by the gills (Brauner et al., 2019; Evans et al., 2005).

In general, the ion-transporting cells (ionocytes) in *A. gigas* gills remain poorly characterized, and the little information that is available is for juveniles >10 g, which is after the transition from water- to air-breathing takes place. Currently, it is known that mitochondrion-rich (MR) cells are present on gill filaments and lamellae of 10-g *A. gigas*, with a proliferation of MR cells in the interlamellar spaces of larger fish, and finally, extensive presence of MR cells in the lamella-lacking filaments of adults (Brauner et al., 2004; Ramos et al., 2013). Immunostaining of *A. gigas* gills also indicates the MR cells are enriched in the enzyme Na^+/K^+-ATPase (NKA) (Brauner et al., 2004; Ramos et al., 2013). However, the enzymatic activity of vacuolar-type H^+-ATPase (VHA) in gills from juvenile and adult *A. gigas* is higher than that of NKA (Pelster et al., 2020; Wood et al., 2020), raising the possibility of different ionocyte characteristics at different life stages which has not previously been investigated.

A number of studies have identified morphological and physiological changes during development in *A. gigas*, 4–6 g or larger, yet little is known about respiratory and ion-regulatory organ development in larvae and early juveniles. After hatch, fish larvae typically respire via the skin and the gills rapidly take on a primary role in ionoregulation (Brauner & Rombough, 2012; Fu et al., 2010). As their surface to volume ratio exceeds the ratio necessary for cutaneous respiration, oxygen uptake shifts to the gills, potentially creating an osmorespiratory–ion regulatory compromise (Sardella & Brauner, 2007). It is thought that in *A. gigas*, this is solved by a period of simultaneous water- and air-breathing, shifting respiration to the accessory ABO. To investigate changes in gill and ABO morphology and physiological characteristics during this transition, *A. gigas* larvae were captured 5–7 days following hatch and reared in the laboratory for 74 days. Fish 4, 10, 21, and 74 days after catch (dac) were chosen for detailed analyses of gills, ABO, and skin.

Taken together, these traits will shed insight into the transition in gas exchange and ionoregulation with increasing dependence upon aerial respiration.

2 MATERIALS AND METHODS

2.1 Rearing and husbandry

Larval *A. gigas* were obtained from a wild-caught broodstock (adults, 1.7–1.8 m length) from a commercial fish farm (Piscigranja Boa Esperança, Rondônia, Brazil). They were captured 5–7 days after hatch when they emerged from the brood nest, and were distributed into two circular 1000-L tanks. Larvae were reared for 74 days in partial flow-through (0.03 $m^3 \cdot s^{-1}$) of well water maintained at 27.9 ± 0.8°C (5.60 ± 0.52 $mg \cdot L^{-1}$ O_2; pH 7.0 ± 0.17; 0.46 ± 0.58 $mg \cdot L^{-1}$ ammonia; 12/12 h light/dark; 900 lx light intensity at the surface). In the first week, larvae were fed ad libitum every 2 h during the day and the feed consisted of 55% live natural zooplankton (78.7% Cladocera, 11.1% Copepoda, and 10.2% Ostracoda) and 45% unenriched *Artemia* (389 individuals/larvae/meal; SepArt cysts; INVE). After 11 days, larvae were switched to a diet of microextruded commercial feed (Aquaxcel Starter WW 4512, 0.8–1.0 mm, 45% crude protein; Cargill) and natural zooplankton diet at night (815 individuals/larva/meal).

This study conforms with the Ethical Committee of Animal Experimentation and Research of the Brazilian National Institute for Research of the Amazon (INPA), Manaus, Amazonas, Brazil (Protocol Number: 016/2016).

2.2 Sampling and histological processing of gills, skin, and ABO for morphometrics

Four age classes of *A. gigas* were selected: 4, 10, 21, and 74 dac (approximately 10, 16, 27, and 80 days post hatch; $n = 3$ per age class). These age classes corresponded to a body mass ranging from 0.07 to 5.45 g (Table 1). *A. gigas* were euthanized with eugenol and fixed in 10% formaldehyde for 24 h before being transferred to 70% EtOH in which they were stored until analyses. Samples were shipped to the University of British Columbia, Canada, for gill and ABO morphometrics.

Table 1. Summary of gill, ABO, and skin dimensions at four different age classes (4, 10, 21, and 74 dac) of juvenile *Arapaima gigas* showing mean ± 95% CI, where applicable

Parameters	Units	4 dac	10 dac	21 dac	74 dac
Body mass	g	0.07 ± 0.005	0.27 ± 0.04	1.64 ± 0.16	5.45 ± 0.26
Body volume	mm^3	46.75	–	1356.74	4643.25
Mean lamellar surface area	mm^2	0.0012	–	0.0019a	0.0019a
Total GSA	mm^2	21.8	–	538.6	2875.5
GSA/body SA		0.05	–	0.27	0.44
Relative lamellar contribution	% of GSA	76	–	71a	52
Filament length	µm	100.02 ± 6.85		829.22 ± 46.57	1051.88 + 51.99
Lamellar length	µm	45.25 ± 3.83	50.78 ± 2.29	58.75 ± 2.02	49.89 ± 1.57
Harmonic mean barrier thickness gills (τ)	µm	1.54 ± 0.2	2.29 ± 0.28	2.40 ± 0.25	4.75 ± 0.59
ADF gills	$mm \cdot g^{-1}$	11.12		1.03a	0.06
Interlamellar cell thickness	µm	11.94 ± 5.78	14.94 ± 5.97	15.72 ± 5.75	29.85 ± 9.39
Skin surface area	mm^2	430.06	–	2027.33	6566.55
τ_{skin}	µm	1.64 ± 0.11	1.84 ± 0.12	2.30 ± 0.10	–
ABO surface area	mm^2	–	–	185.08	559.76
ABO volume	mm^3	–	–	28.69	113.31
ABO/body volume		–	–	0.14	0.02
τ_{ABO}	µm	–	–	10.03 ± 1.84	10.23 ± 1.82

Parameters	Units	4 dac	10 dac	21 dac	74 dac
ADF_{ABO}	$mm \cdot g^{-1}$	–		11.24	10.03

- Abbreviations: ABO, air-breathing organ; ADF, anatomical diffusion factor; CI, confidence interval; dac, days after catch; GSA, gill surface area.
- [a] At 15 dac.

2.2.1 Gills

Whole gill baskets were removed from one side of the fish and each of the four gill arches were dissected out. Each gill arch was photographed under a stereo microscope (Olympus SZX10 stereoscope with a DP72 camera) and all filaments on each gill arch were measured for length, distance on gill arch along with the total length of the arch. The second gill arch from each fish was embedded in Spurr's resin, following dehydration, and cut transversely at 1 µm with an automated ultramicrotome (Leica Ultracut 7) with a diamond knife. Every 10th section was collected, stained with Toluidine blue and photographed at different magnifications (×10 air to ×64 oil immersion) with a microscope-mounted camera (Zeiss Axioplan Fluorescent Microscope). After serial sectioning, the total number of sections was divided by 10 equally distanced sections that were used for determining gill dimensions. Lamellar length was measured from the base of the filament to the tip for all lamellae in the section. Lamellar length was cross-validated from confocal images described below. To determine water–blood diffusion distances (l_h), a Merz grid was overlaid and distance between the outer epithelium and the nearest capillary (visible by erythrocytes) was measured on intersecting points and corrected for magnification (Howard & Reed, 2004; Perry, 1978). The harmonic mean barrier thickness (τ) was calculated as $\tau = 2/3\ l_h$ (Weibel & Knight, 1964).

On a subset of two samples, vertical random uniform (VUR) sections were prepared and cut and compared with the transverse sections. After determining consistency in results between transverse and VUR sections, the VUR method was discontinued as it yielded the same information but was much more time consuming on the ultramicrotome. For determining gill surface area, gill filaments from the third gill arch were rehydrated, cleared with FocusClear™ (Cedarlane®) and imaged in three dimensions (3D) by autofluorescence using laser scanning/two-photon confocal microscopy (Olympus FV1000, ×25/NA 1.05; WD 2 mm, Spectra-Physics MaiTai laser [690–1000 nm] with DeepSee dispersion compensation unit). Confocal images were analyzed with the 3D microscopy software Amira (Thermo Fisher Scientific) by overlaying a triangular grid and computing surface area. Respiratory surface area (S_R) was quantified by measuring the surface area of the lamellae only. The anatomical diffusion factor (ADF) was then calculated by dividing the S_R relative to body mass by τ (Perry, 1978).

2.2.2 Skin

To determine the blood–water diffusion distance of the skin, three fish per age group were embedded in Spurr's resin, following dehydration, and cut dorso-ventrally in 1-µm sections on an automated ultramicrotome (Leica Ultracut 7) with a diamond knife. Three random sections were stained with Toluidine blue and imaged at ×64 oil immersion with a microscope-mounted camera (Zeiss Axioplan Fluorescent Microscope). Twenty measurements were taken from each of these three sections from the outermost layer of the epidermis to the nearest capillary (visible by erythrocytes) using the image analysis software ImageJ©.

2.2.3 ABO

To determine the air–blood diffusion distances in the ABO, 1-cm-thick sections through the ABO of whole fixed *A. gigas* were dehydrated, embedded in wax, and cut on a microtome at 5-µm sections. These sections were stained with hematoxylin and eosin (H&E) and imaged on a light microscope at ×10. To determine the surface area and volume of the ABO, whole *A. gigas* were scanned with a micro-computed

tomography (micro-CT) as described below. The τ and ADF were calculated for the ABO as described above for gills.

2.3 CT scanning of ABO for 3D imaging

Samples of three size classes of *A. gigas* (4, 21, and 74 dac) were shipped to Aarhus University, Denmark, for micro-CT scans. Imaging was performed using two systems to acquire high-resolution three-dimensional information of body dimensions and ABO anatomy. For the two smallest samples a Scanco Medical µCT50 system (Scanco Medical) was used with 2000 projections/180°, an isotropic voxel size of 6.8 µm (4 dac) or 14.8 µm (21 dac), an X-ray tube voltage of 70 kVp, an X-ray tube current of 342 µA, and an integration time of 3000 ms and applying a 0.5-mm aluminum filter. For the largest sample (74 dac) a Scanco Medical XtremeCT system (Scanco Medical AG) was used with 1500 projections/180° and an isotropic voxel size of 41 µm, an X-ray tube voltage of 59.4 kVp, an X-ray type current of 119 µA, and an integration time of 132 ms.

Volume and surface area of body and ABO were estimated from the micro-CT scans using stereological principles (Mühlfeld et al., 2010). In short, volume and surface area were estimated by randomly selecting animal orientation in the scanner and then choosing 12 equally spaced parallel sections spanning either the air sac or the entire body and then applying a systematic uniform point grid (for volume estimation) or a systematic set of parallel test lines (for surface area estimation) on each section plane. Volume was calculated by counting the number of test points intersecting either the ABO or body using the Cavalieri estimator (Howard & Reed, 2004; Perry, 1978). Surface area was calculated by counting the number of intersections of test lines with the exterior surface of the ABO or the body surface.

2.4 Immunoblotting, immunohistochemistry, and gill ionocyte quantification

2.4.1 Antibodies

NKA was immunodetected using α5, a mouse monoclonal antibody raised against the α-subunit of chicken NKA (a5, Developmental Studies Hybridoma Bank; Lebovitz et al., 1989). This antibody specifically recognizes NKA α-subunits from diverse elasmobranch and teleost fishes including leopard shark (*Triakis semifasciata*; Roa et al., 2014; Roa & Tresguerres, 2017), yellowfin tuna (*Thunnus albacares*; Kwan et al., 2019), coho salmon (*Oncorhynchus kitsutch*; Wilson et al., 2002), blue-green damselfish (*Chromis viridis*; Tang et al., 2014), giant mudskipper (*Periophthalmodon schlosseri*; Wilson et al., 2000), Pacific Chub Mackerel (*Scomber japonicus*; Kwan et al., 2020), among others. VHA was immunodetected using custom-made rabbit polyclonal antibodies against a conserved epitope in the B subunit (AREEVPGRRGFPGY; GenScript). These antibodies specifically recognize VHA from diverse invertebrates (Barott et al., 2015; Hill et al., 2018; Tresguerres et al., 2013) and vertebrates (Kwan et al., 2020; Roa et al., 2014; Roa & Tresguerres, 2017). The secondary antibodies used in this study include goat anti-mouse IgG-HRP and goat anti-rabbit IgG-HRP conjugate (Bio-Rad) for Western blot analysis, and goat anti-mouse Alexa Fluor 546, goat anti-rabbit Alexa Fluor 488 (Invitrogen) for immunohistochemistry.

The specificity of the NKA and VHA antibodies in *A. gigas* was verified through Western blot analysis of gill tissue following the methods described in Kwan et al. (2020) and described in detail in Supporting Information File S1. Both NKA and VHA yielded single bands of the expected sizes: ~100 and ~53 kDa, respectively (Figure S1A). For VHA, no signal was detected in either Western blot analysis or immunohistochemistry following the peptide pre-absorption treatment (1:5 antibody to peptide ratio on a molar basis; pre-incubated overnight at 4°C on shaker) (Figure S1A–C).

2.4.2 Whole-mount immunohistochemistry

Fixed *A. gigas* larvae and excised adult gill tissues were prepared at room temperature as follows. Washed in phosphate-buffered saline (PBS) + 0.1% Tween (PBS-T) for 5 min, rinsed in ice-cold PBS with sodium borohydride (1.0–1.5 mg·ml^{-1}; six times, 10 min each), incubated in blocking buffer (PBS-T, 0.02% normal goat serum, 0.0002% keyhole limpet hemocyanin) for 1 h, and with the primary antibodies (NKA: 40 ng·ml^{-1}; VHA: 6 µg·ml^{-1}) overnight. On the following day, samples were washed in PBS-T (three times, 10 min each), and incubated with fluorescent secondary antibodies (1:500) and counterstained with 4′,6-diamidino-2-phenylindole (DAPI) (1 µg·ml^{-1}) for 1 h. Samples were washed in PBS-T (three times, 10 min each), and imaged on an inverted confocal microscope (Zeiss LSM 800 with Zeiss ZEN 2.6 blue edition software).

2.4.3 Ionocyte quantification

Following whole-mount immunostaining and imaging, ionocyte density was estimated from the leading and trailing edges of both filaments and lamellae across four developmental stages: 4, 10, 21, 74 dac, and adult ($n = 3$ per stage). The number of NKA- and VHA-rich ionocytes on gill filament and lamellae were manually counted, and the filament and lamellae surface area were estimated using Fiji (Schindelin et al., 2012). Ionocyte density was calculated by dividing ionocyte count by its respective surface area.

2.5 Statistical analysis

All statistical analyses were performed in the open-access program R© (R Core Team, 2018). Gill, ABO, and skin dimensions, such as lamellar length, barrier thickness, and surface area, were compared between age groups using a one-way analysis of variance (ANOVA) and Tukey's honestly significant difference posthoc test with the package DescTools (Signorell et al., 2020). Ionocyte density were compared across age groups and gill edges (leading, trailing) using two-way ANOVA and Tukey's multiple comparisons posthoc test.

3 RESULTS

3.1 Gills

3.1.1 Morphometrics

Gills were analyzed from *A. gigas* at 4, 10, 21, and 74 dac (approximately 10, 16, 27, and 80 days post hatch) which correspond to a body mass ranging from 0.07 to 5.45 g wet weight (from formalin-fixed samples) and a total length of 23–94 mm. Histological sections of gill filaments and lamellae revealed a decrease in lamellar length concurrent with an increase in diffusion distance and significant thickening of filaments and the appearance of interlamellar cells between 21 and 74 dac (Figure 1). Until 21 dac, the gills of juvenile *A. gigas* possess clearly visible lamellae, that become stubbier beyond that age and lamellar length was significantly greater at 21 dac than all other age groups ($F_3 = 22.5$; $p < 0.0001$; Figure 2a and Table 1). Filament lengths increased throughout development, with an eightfold increase from 4 to 21 dac (Figure 2b and Table 1), while the gill arch length increased 10-fold between 21 and 74 dac. Gill arch 3 had the longest gill filaments in all developmental stages analyzed, while gill filaments on arch 1 were progressively reduced relative to the other gill arches, from 4 to 74 dac. The mean number of lamellae per millimeter filament (one side) was 20 ± 4 lamellae and did not differ significantly ($p = 0.216$) between age groups. The distance between lamellae increased significantly between 10 and 21 dac from 25.7 (±11.1) µm to 30.6 (±9.0) µm, and between 21 and 74 dac to 40.4 (±12.1) µm ($p < 0.0001$).

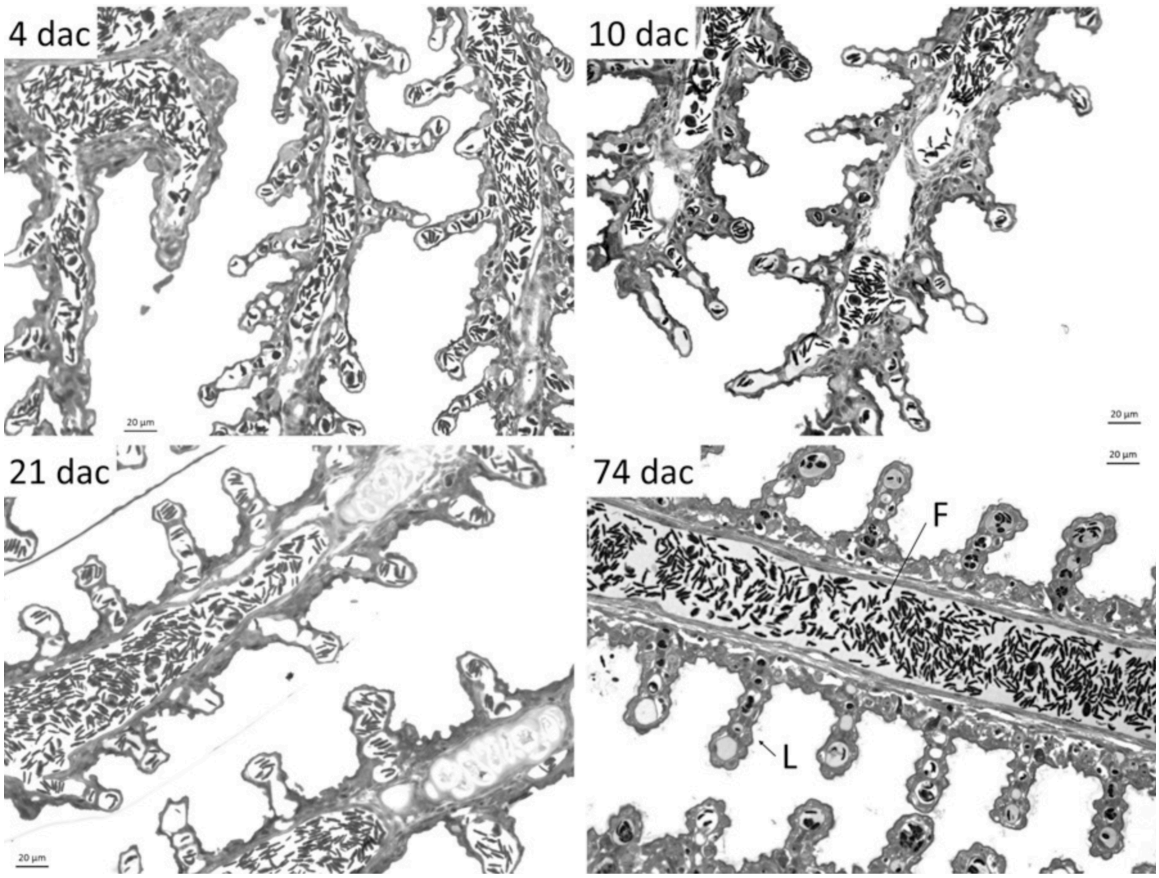

Figure 1 Representative transverse histological sections of gills of juvenile *Arapaima gigas* at 4, 10, 21, and 74 days after catch (dac). Lamellae (L), filament (F), interlamellar cell thickness. One-micrometer-thick methacrylate sections, hematoxylin and eosin, ×100 light microscopy

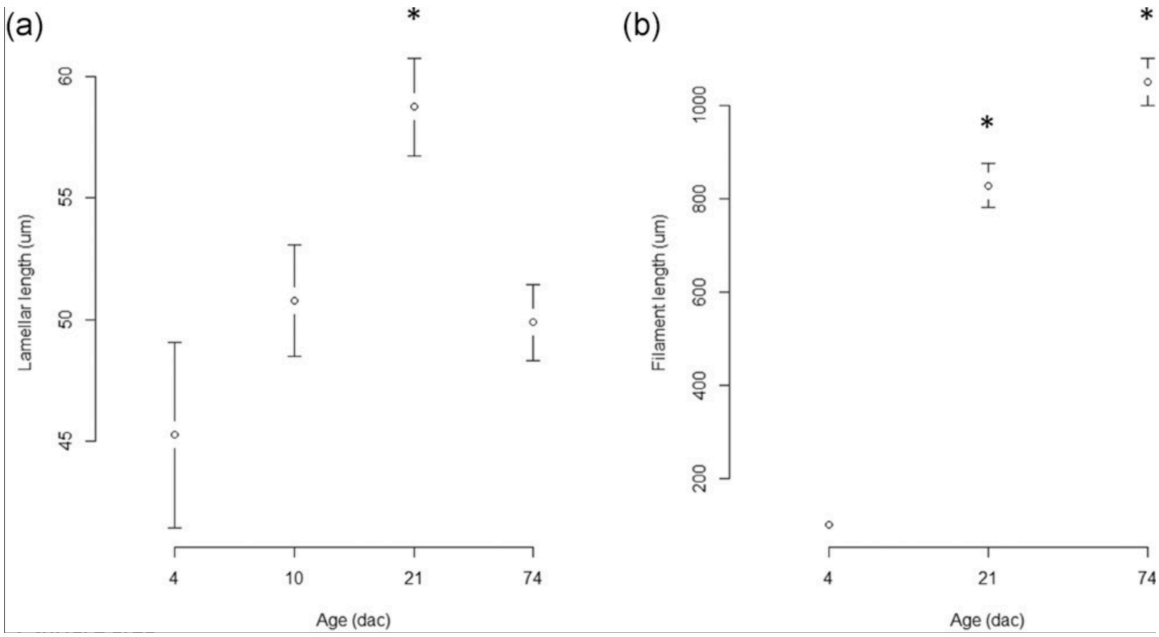

Figure 2 Changes in mean (±confidence interval) of (a) lamellar length and (b) filament length of gills of *Arapaima gigas* throughout development from 4 ($N = 23$; 120), 10 ($N = 66$), 21 ($N = 80$; 193), and 74 ($N = 113$; 244) days after catch (dac); (N = number of samples of lamellae; filaments). *Significant differences $p < 0.001$

3.1.2 Surface area

Analysis of gill surface area from confocal imaging (Figure 3a) revealed an increase in total gill surface area relative to body mass throughout development; however, the relative respiratory gill surface area decreased between 15 and 74 dac (Table 1). The relative lamellar contribution to total gill surface area remained above 70% in juveniles up to 15 dac, but decreased to 52% by 74 dac, which was driven by the 18% decrease in lamellar length during this developmental period. Whole gill surface area scaled allometrically with body size with an exponent of 1 between 4 and 21 dac, and 1.4 between 21 and 74 dac. However, respiratory surface area (lamellar area only) scaled hypoallometrically to body mass by 0.2 between 4 and 15 dac and by −0.1 between 15 and 74 dac, showing a decrease in relative respiratory gill surface for the later developmental stages.

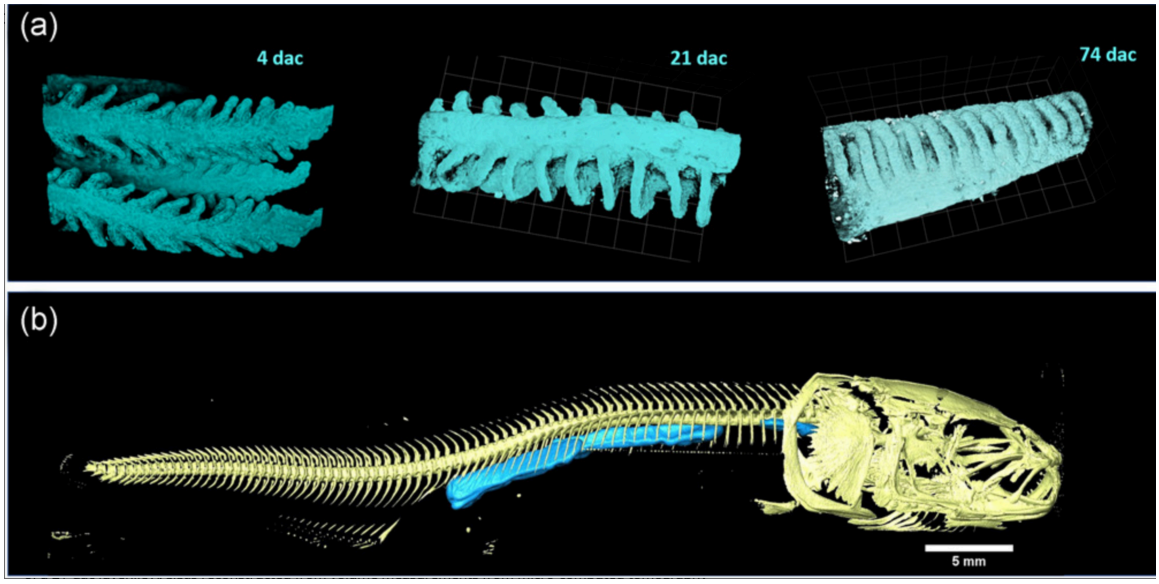

Figure 3 (a) Representative confocal images of gill filaments and lamellae of juvenile *Arapaima gigas* at 4, 21, and 74 days after catch (dac) for surface area analysis using self-fluorescence at ×10 magnification. (b) Lateral view of a 21-dac juvenile *A. gigas* reconstructed from volume measurements from micro-computed tomography scanning. Blue represents the air-breathing organ, yellow indicates bone

3.1.3 Diffusion distance

The harmonic mean barrier thickness (τ) of the gills increased significantly between 21 and 74 dac by 50% ($p < 0.0001$) (Figure 4a), while the interlamellar cell thickness also increased significantly by 50% ($p < 0.0001$). The ADF of the gills, representing the capacity for gas exchange, decreased 10-fold between 4 and 15 dac and a further 16-fold between 15 and 74 dac.

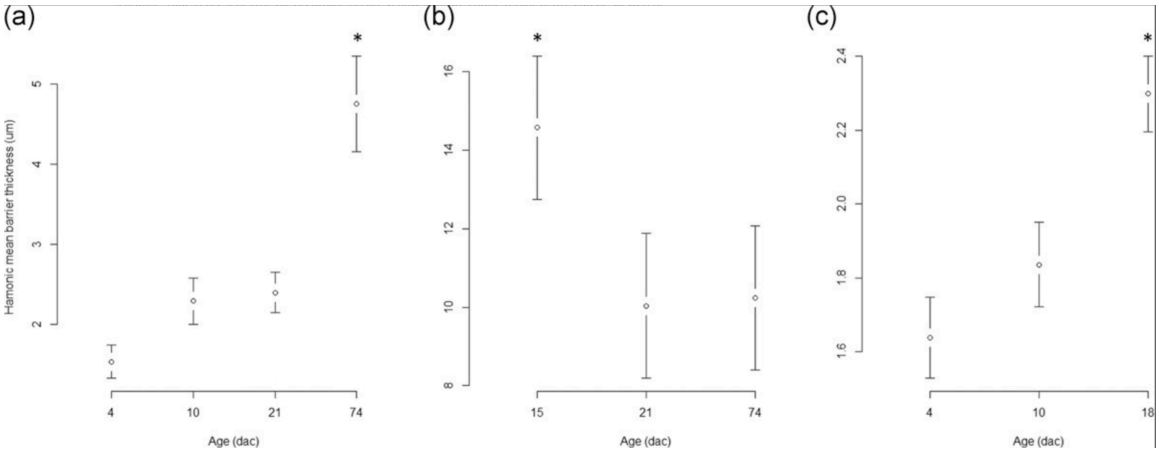

Figure 4 Changes in mean (±confidence interval) of harmonic mean barrier thickness of (a) gills ($N = 83–171$), (b) air-breathing organ ($N = 18–21$) and (c) skin ($N = 180–240$), throughout developing *Arapaima gigas* from 4 to 74 dac; $N = 83–240$. *Significant differences

3.2 ABO

The swim bladder was apparent at 4 dac and developed into a well-defined ABO by 21 dac (Figure 5), with the parenchyma beginning to develop edicular air spaces as the ABO was fused with the vertebrae and kidneys (Figure 6). In 74-dac fish, collagen was visible in the parenchyma and the ABO developed the convoluted structure typical of adult air-breathing *A. gigas*. The swim bladder/ABO of 4- and 10-dac juveniles were very small and prevented accurate estimation of their surface and volume. There was a fivefold increase in total ABO surface area between 21 and 74 dac (Table 1), resulting in a scaling exponent of ABO to body mass of 0.9. The effective respiratory surface area of the ABO could not be accurately estimated due to the highly convoluted nature of the parenchyma (Figure 6). The harmonic mean barrier thickness of the ABO decreased by 30% from 15 to 21 dac but remained constant between 21 and 74 dac (Figure 4b).

Figure 5 Cross-section of the body cavity of juvenile *Arapaima gigas* showing the swim bladder modified to an air-breathing organ (ABO) during development from water- to air-breathing: (a) 4 dac (b) 9 dac, and (c) 21 dac. Swim bladder (sb); ABO (ab), centrum (c), intestine (i), kidney (k), muscle (m), parenchyma (p), vertebra (v). Note that magnification is the same in every image. Five-micrometer-thick wax section, hematoxylin and eosin, ×10 light microscopy

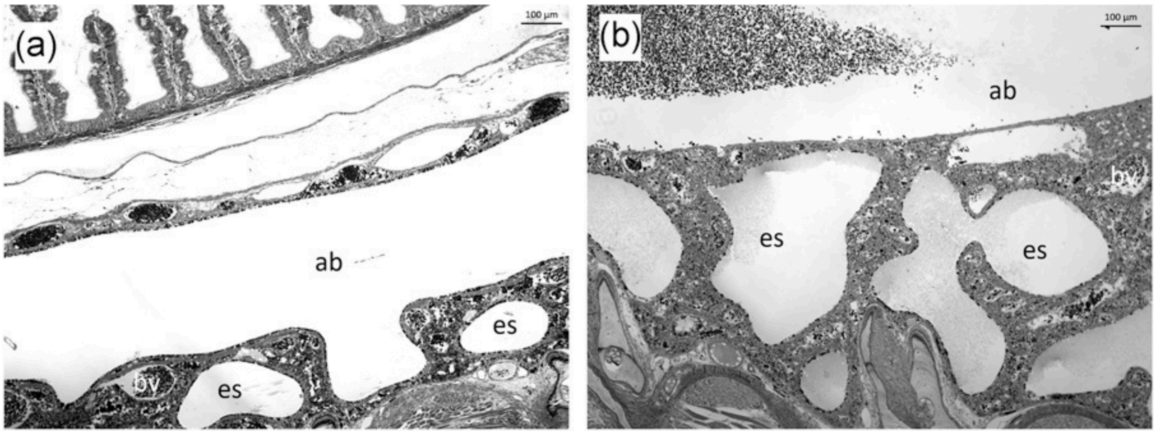

Figure 6 Respiratory region (parenchyma) of the air-breating organ (ab) of juvenile *Arapaima gigas* at two developmental stages: (a) 21 dac, (b) 74 dac. Edicular air spaces (es), large blood vessels (bv), collagen (c). One-micrometer-thick methacrylate section, Toluidine blue, ×10 light microscopy

3.3 Skin

Between 4 and 21 dac, the skin surface area to volume ratio of juvenile *A. gigas* decreased from 9 to 1.5 where it remained constant until 74 dac (Table 1). Relative skin surface area to body weight declined over development, scaling hypoallometrically with an exponent of −0.4 from 4 to 74 dac. Concurrently, the dermis thickened resulting in an increase in water–blood diffusion distance from 2.5 to 3.5 µm, similar to the barrier thickness of the lamellae at these developmental stages (Table 1). The harmonic mean barrier thickness increased significantly by 20% between 10 and 18 dac (Figure 4c). Goblet cells first appear in the skin at 15 dac and remained present onward.

3.4 Ionocytes

Based on NKA and VHA immunostaining, *A. gigas* up to 2 g (4–21 dac) had one type of gill ionocyte that abundantly expressed both enzymes. Z-stack reconstructions of confocal images reveal NKA was present in the highly infolded basolateral membrane, whereas VHA was present in the apical membrane (Figure 7a–c). This NKA-rich ionocyte was observed on both the leading and trailing edge of the gill filament and lamellae (Figure S2). This ionocyte type was also observed in larger *A. gigas* (74-dac juveniles and adults); however, VHA was observed to be in the subapical area rather than in the apical membrane itself (Figure 7d,e). Additionally, the larger *A. gigas* expressed a second gill ionocyte type that expressed abundant VHA but had no detectable NKA signal (Figure 7d,f). Z-stack reconstruction images indicated VHA was present in the basolateral membrane of VHA-only ionocytes (Figure 8f). VHA-only ionocytes were found on both the leading and trailing edge of the filament, and they were never observed on lamellae (Figure S3).

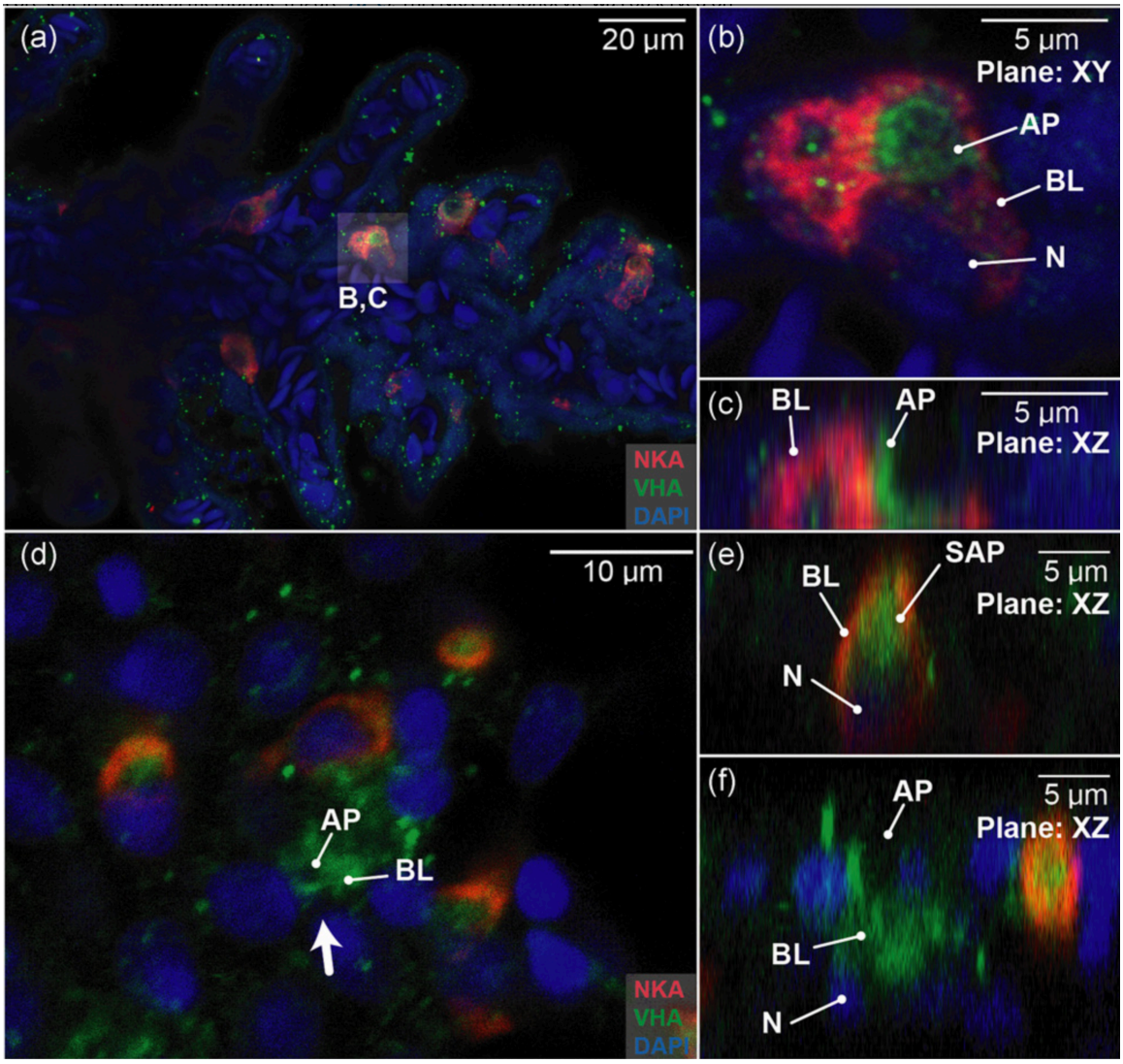

Figure 7 Gill ionocytes in *Arapaima gigas* identified by Na^+/K^+-ATPase (NKA) and vacuolar-type H^+-ATPase (VHA) immunostaining. (a) Gills from 4-dac fish (~0.1 g) had a single type of ionocyte expressing both NKA and VHA. (b, c) Higher magnification and Z stacks showed NKA and VHA in the basolateral and apical membranes, respectively. (d) In contrast, gills from adult *A. gigas* had two types of ionocytes: (d, e) the first type of ionocyte had basolateral NKA and subapical VHA, (d, f) whereas the second type contained basolateral VHA and lacked NKA. AP, apical membrane; BL, basolateral membrane; N, nucleus, SAP, sub-apical membrane. NKA is in red, VHA is in green, and nuclei are in blue.

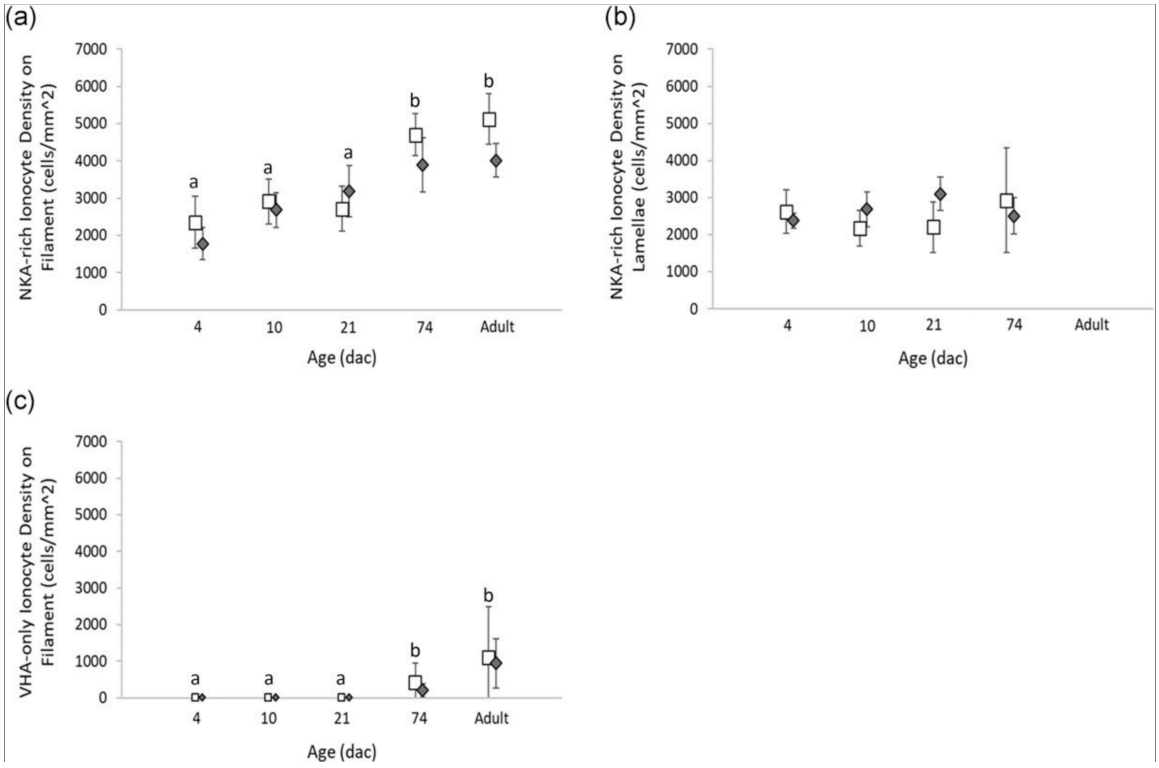

Figure 8 Ionocyte density in gills from juvenile and adult *Arapaima gigas*. (a) Na^+/K^+-ATPase-rich (NKA-rich) ionocytes on gill filaments. (b) NKA-rich ionocytes on gill lamellae. (c) Vacuolar-type H^+-ATPase (VHA)-only ionocytes on gill filaments. The letters denote significant differences between developmental stages. $N = 3$ fish per age class. Error bars denote *SD*

The density of NKA-rich ionocytes in the gill filament significantly increased throughout development ($p < 0.0001$), and 74-dac juvenile and adult *A. gigas* had significantly higher densities than the younger juveniles (Figure 8a). In contrast, the density of the NKA-rich ionocytes in the lamellae did not change between 4 and 72 dac ($p = 0.7915$; Figure 8b) (the gills of adult *A. gigas* lacked lamellae). As mentioned above, VHA-only ionocytes were first observed in 74-dac fish. The density of these ionocytes tends to increase in adult *A. gigas* gills; however, the differences were not significantly different ($p = 0.1760$; Figure 8c). Finally, there were no significant differences in the density of either ionocyte type between the leading and trailing edges of filaments and lamellae across developmental stages (Figure 8a–c).

4 DISCUSSION

Here, we elucidate developmental steps in the transition from water- to air-breathing in the obligate air-breather *A. gigas* by analyzing changes in the gills, swim bladder (modified to the ABO), and skin for gas exchange and ion regulation in the gills. We quantified morphological changes, surface area, and barrier thicknesses in the gills, ABO, and skin and determined ionocyte types and abundance in the gills. Our data show that up until about 4 weeks of age (21 dac, ~1.6 g body mass) the gills and skin of *A. gigas* appear similar to water-breathing fish, in terms of morphology, surface area, and diffusion distance. Between 4 and 11 weeks (74 dac, ~5.5 g), there is a distinct shift in which gills are reduced and the dermis thickens, while the ABO increases in size and complexity, likely indicating a trimodal breathing phase in this stage.

Microscopical analyses of gill structure revealed significant changes in gill morphology throughout development from 1 to 11 weeks post hatch. Between 1 and 4 weeks post hatch (4–21 dac) the length of lamellae increased by 20%, after which decreased again by 15% by 11 weeks post hatch (74 dac). Thus development between 1.6 and 5.5 g marks the transition from lamellar expansion to lamellar reduction, leading to the stubby appearance of lamellae at 10 g and their complete disappearance observed in 1-kg adult *A. gigas* (Brauner et al., 2004).

The number of lamellae did not change throughout development in *A. gigas* and we found a mean 20 ± 4 lamellae per millimeter filament (one side), consistent with what has been reported for *A. gigas* up to 200 g (Ramos et al., 2013). After 500 g body mass, lamellar structures have been shown to decrease significantly reaching 14 lamellae per millimeter filament in 5-kg fish (Ramos et al., 2013); therefore, lamellar reduction is primarily accomplished by a decrease in lamellar size, not number. Filament length continuously increased with development, indicating a likely role other than oxygen uptake.

A tissue's effectiveness for gas exchange is driven mainly by the surface area available and the diffusion thickness between the environment and the blood. Gill surface area in young *A. gigas* was consistent with that observed in other water-breathing fish until about 4 weeks (21 dac, 1.6 g) where gill surface area scaled to body mass with an exponent of 1, similar to water-breathing fish and the air-breathing *Pangasianodon hypophthalmus* (Phuong et al., 2018). At 4 weeks (21 dac), the gill surface area in *A. gigas* was ~27% of the total body surface area, with a ~70% lamellar contribution. Larval chinook salmon (*Oncorhynchus tshawytscha*) are able to supply ~60% of their oxygen uptake via the gills with a comparable gill to total body surface ratio (Rombough & Ure, 1991), suggesting a strong capacity for branchial respiration in *A. gigas* during this phase. Between 4 and 11 weeks (21, 1.6, and 74 dac, 5.5 g, respectively), the lamellar surface area decreased by 20%, thus decreasing the relative effective respiratory area.

At the same time, the diffusion distance of the lamellae and the thickness of the interlamellar spaces in the filaments increased by ~50%, decreasing the capacity for branchial gas exchange. The harmonic mean barrier thickness (τ) increased fourfold from 1 to 11 weeks (mean $\tau = 1.5$ µm at 0.07 g, 4 dac to $\tau = 4.75$ µm at 5.5 g, 74 dac) resulting in an ADF decreasing from 11 to 0.06 $mm \cdot g^{-1}$ for this size range. The increase in ADF signifies the decreased capacity of the gills for oxygen uptake. By 100 g, the fully air-breathing *A. gigas* have a τ of 7.76 µm with an ADF orders of magnitude lower (0.099 $cm^2 \cdot \mu m^{-1} \cdot g^{-1}$) (Da Costa et al., 2007). These gill modifications likely aid in preventing O_2 loss via the gills in hypoxic water (Cameron & Wood, 1978; Pelster & Wood, 2018). It is likely, that at 1.6 g (21 dac) *A. gigas* can still supply most of their oxygen needs through aquatic respiration, while at 5.5 g (74 dac) they use their gills mainly for CO_2 and nitrogen waste excretion (Pelster et al., 2020).

Fish embryos and larvae rely on cutaneous gas exchange before the onset of gill lamellae. Early in development, gills are considered the main site of ion regulation, having extensive mitochondria-rich cells, or ionocytes, before the development of respiratory lamellar structures (Rombough, 2002). As the fish grows and gills develop, larvae undergo a bimodal phase in which they rely on cutaneous bulk gas diffusion coupled with branchial respiration. In larval salmonids >80% of oxygen requirements are met cutaneously (Rombough & Ure, 1991), while the gills become the predominant site of gas exchange after a body mass of 2.5–5 g (Rombough & Moroz, 1990). In our study, the relative skin surface area to body weight decreased allometrically with an exponent of −0.4 throughout the developmental range analyzed (4–74 dac). Additionally, in fishes relying on cutaneous breathing, thin epithelia and high capillary perfusion are necessary requirements for effective oxygen diffusion. The harmonic mean barrier thickness of the skin in 1-week-old *A. gigas* was similar to that of the gills ($\tau = 1.6$) and increased at a rate comparable to the gills of about 20% per week. At 3 weeks (15 dac, 0.8 g) goblet cells first appeared and the skin started taking on the distinctive armoured appearance of the adult *A. gigas*. The simultaneous thickening of skin and gill epithelia together with the reduction of gill lamellae serve to prevent O_2 loss from the blood into hypoxic water by diffusion across permeable surfaces.

Interestingly, the harmonic mean barrier thickness of the ABO decreased at a faster rate of ~30% between 3 and 4 weeks of age (15 and 21 dac, 0.77 and 1.6 g, respectively). The modification of the ABO to an ABO

in *A. gigas*, and the reduction in barrier thickness promotes oxygen uptake across the ABO which is especially beneficial when living in the routinely hypoxic waters of the Amazon.

The swim bladder in early *A. gigas* was not morphologically different to that of a water-breathing fish. Modifications toward the accessory ABO commenced around 0.2 g (9 dac), with the first parenchyma structures appearing wrapped around the kidneys. At 1.6 g (21 dac) the ABO had a complex and convoluted structure, extending far along the vertebrae with edicular sacs perfused with blood vessels. Between 1.6 and 5.5 g, the ABO increased fivefold in volume and the parenchyma greatly increased in complexity, increasing the effective respiratory surface area of the ABO. A recent study has shown that at 4–6 g, juvenile *A. gigas* already cover 63% of their O_2 requirements from the air using their modified ABO (Pelster et al., 2020). Our study is consistent with this finding, where gill and ABO modifications support the hypothesis that the transition from water- to air-breathing likely commences after 1 g body mass (~3 weeks post hatch) at the time at which this life stage has been observed swimming to the surface to take air-breaths (Graham, 1997; Lüling, 1964).

As breathing shifts to the ABO, the gills appear to take on a greater role in ion regulation, seen in the proliferation of NKA- and VHA-rich ionocytes in the filaments, that were similar in density in gills of 74 dac to adult fish. Younger fish up to 1.6 g (21 dac) had only one gill ionocyte type, which abundantly expressed both NKA and VHA. The NKA signal filled up almost the entire ionocyte, indicating NKA is present in the extensive basolateral infoldings of *A. gigas* gill MR cells (Ramos et al., 2013). On the contrary, the VHA signal was clearly present on the apical membrane, with a pattern that resembled the short microvilli identified in *A. gigas* gill cells by scanning electron microscopy (Ramos et al., 2013). These patterns indicate that NKA- and VHA-rich ionocytes likely excrete H^+ into the water via apical VHAs, and absorb Na^+ into the blood via basolateral NKAs as proposed for other fishes living in ion-poor and acidic water (Parks et al., 2008). We predict these ionocytes also have apical Na^+ channels, as shown in rainbow trout (Dymowska et al., 2014); an area of interest for further investigation.

NKA- and VHA-rich ionocytes were also present in larger *A. gigas*. However, the VHA signal was diffuse on the subapical region rather than directly on the apical membrane, suggesting VHA was stored in vesicles. Importantly, the water in the holding tanks used in this study had pH ~7, and larger fish with reduced ion permeability may not require VHA to excrete H^+ to permit Na^+ uptake under these conditions. Future research should investigate whether VHA inserts into the apical membrane during conditions that require an upregulation of H^+ excretion such as intensive exercise, hypoxia, hypercapnia, or acidic water.

The gills of 72-dac juveniles and those of adult *A. gigas* had a second ionocyte type with strong VHA signal in its basolateral membrane and without detectable NKA signal. We tentatively propose this cell is involved in H^+ and Cl^- absorption and HCO_3^- excretion as established for marine elasmobranchs (Roa et al., 2014; Tresguerres et al., 2005) and proposed for some freshwater fishes (Tresguerres et al., 2006). If this proposition is correct, the VHA-only ionocyte should have anion exchangers (or perhaps cystic fibrosis transmembrane conductance regulator [CFTR] channels) on its apical membrane to be able to excrete HCO_3^- into the surrounding water. Interestingly, the VHA-only ionocyte appeared in larger *A. gigas*, which are more reliant on aerial respiration and have elevated blood CO_2 and HCO_3^-. The VHA-only ionocyte identified in the current study is a promising candidate for this role.

As *A. gigas* grows larger, the gill lamellae become shorter and are eventually lost. The increase of NKA- and VHA-rich ionocyte density on the gill filament during development reflects the continued need for gill ion-transporting processes as the gill total surface area becomes reduced. Likewise, ionocytes are typically present at the trailing edge of fish gills (Evans et al., 2005), so their presence at both the leading and trailing edges of *A. gigas* of all ages maximizes the gill capacity for ion transport in the ion-poor Amazonian environment. Interestingly, unidirectional Na^+ uptake rates are higher in larger *A. gigas* (700 g) than smaller *A. gigas* (70 g (Gonzalez et al., 2010) and 20 g (Pelster et al., 2020)), despite lower gill tissue NKA activity in the larger fish (Gonzalez et al., 2010), but both are relatively low in comparison with water-breathing fish. Gill tissue V-type H^+ ATPase activity was three to four times higher than gill NKA activity in 20- and 600-g fish (Pelster et al., 2020), but did not differ between the size groups. The gills of *A. gigas* appear to be relatively insensitive to low water pH where water pH values as low as pH of 3.5 only result in a modest

increase in Na^+ loss making them one of the most acid-resistant species investigated (Gonzalez et al., 2002).

5 CONCLUSION

Our results provide novel insights on the early transition from water- to air-breathing, as well as potential cellular mechanisms for blood acid–base regulation during development in *A. gigas*.

We show that most of the changes associated with the transition from water- to air-breathing appear to occur between 1.6 and 5 g body mass, corresponding to about 4 and 11 weeks of age. During this transition, lamellar surface area is reduced and the dermis thickens, while the ABO increases in size and complexity, as the diffusion barrier is reduced, likely indicating a trimodal breathing phase. Finally, we identified the presence of two ionocyte types in *A. gigas* gills. The first type likely excretes H^+ and takes up Na^+ and seems to be more active in fish up to 1.6 g, while the second type putatively absorbs H^+ and Cl^- and excretes HCO_3^- and was only detected in fish >5 g. Increased ionocyte density on gill filaments in both the leading and trailing edges reflect compensatory responses to maintain ion-transporting functions while reducing gill surface area. The changes quantified in this study highlight many areas for further study in one of the most obligate air-breathing fishes known.

ACKNOWLEDGMENTS

The authors would like to thank Maria de Nazare Paula da Silva for helping to facilitate lab work and Kevin Hodgson for his assistance with confocal imaging. This study was funded by a Natural Sciences and Engineering Research Council Discovery grant (RGPIN 2018-04172) to Colin J. Brauner and the National Science Foundation IOS 1754994 to Martin Tresguerres. This study is part of INCT-ADAPTA, supported by Brazilian National Research Council (CNPq 465540/2014-7), Amazonas State Research Foundation (FAPEAM; 062.1187/2017), and the Brazilian Higher Education Improvement (CAPES; finance code 001) to Adalberto L. Val.

CONFLICT OF INTERESTS

The authors declare that there are no conflict of interests.

DATA AVAILABILITY STATEMENT

The data that support the findings of this study are available on request from the corresponding author.

References

-Barott, K. L., Perez, S. O., Linsmayer, L. B., & Tresguerres, M. (2015). Differential localization of ion transporters suggests distinct cellular mechanisms for calcification and photosynthesis between two coral species. *American Journal of Physiology-Regulatory, Integrative and Comparative Physiology*, 309(3), R235– R246.

-Brauner, C. J., & Berenbrink, M. (2007). Gas transport and exchange. *Fish Physiology*, 26, 213– 282.

• Brauner, C. J., & Rombough, P. J. (2012). Ontogeny and paleophysiology of the gill: New insights from larval and air-breathing fish. *Respiratory Physiology & Neurobiology*, 184(3), 293– 300.

• Brauner, C. J., Shartau, R., Damsgaard, C., Esbaugh, A., Wilson, R., & Grosell, M. (2019). Acid-base physiology and CO_2 homeostasis: Regulation and compensation. In M. Grosell, P. L. Munday, A. P. Farrell, & C. J. Brauner (Eds.), Fish physiology (Vol. 37). Academic Press.

• Brauner, C. J., & Val, A. L. (1996). The interaction between O_2 and CO_2 exchange in the obligate air breather, *Arapaima gigas*, and the facultative air breather, *Lipossarcus pardalis*. In A. L. Val, V. M. F. Almeida-Val, & D. J. Randall (Eds.), Physiology and biochemistry of the fishes of the Amazon (pp. 101–110). INPA.

• Cameron, J. N., & Wood, C. M. (1978). Renal function and acid-base regulation in two Amazonian erythrinid fishes: *Hoplias malabaricus*, a facultative air breather. *Canadian Journal of Zoology*, 56, 917–930.

• Da Costa, O. T. F., Pedretti, A. C. E., Schmitz, A., Perry, S. F., & Fernandes, M. N. (2007). Stereological estimation of surface area and barrier thickness of fish gills in vertical sections. *Journal of Microscopy*, 225(1), 1– 9.

• Dymowska, A. K., Schultz, A. G., Blair, S. D., Chamot, D., & Goss, G. G. (2014). Acid-sensing ion channels are involved in epithelial Na^+ uptake in the rainbow trout *Oncorhynchus mykiss*. *American Journal of Physiology-Cell Physiology*, 307(3), C255– C265.

• Evans, D. H., Piermarini, P. M., & Choe, K. P. (2005). The multifunctional fish gill: Dominant site of gas exchange, osmoregulation, acid-base regulation, and excretion of nitrogenous waste. *Physiological Reviews*, 85(1), 97– 177.

• Fernandes, M. N., da Cruz, A. L., da Costa, O. T. F., & Perry, S. F. (2012). Morphometric partitioning of the respiratory surface area and diffusion capacity of the gills and swim bladder in juvenile Amazonian air-breathing fish *Arapaima gigas*. *Micron*, 43(9), 961– 970.

• Fu, C., Wilson, J. M., Rombough, P. J., & Brauner, C. J. (2010). Ions first: Na^+ uptake shifts from the skin to the gills before O_2 uptake in developing rainbow trout, *Oncorhynchus mykiss*. *Proceedings of the Royal Society B: Biological Sciences*, 277(1687), 1553– 1560.

• Gonzalez, R. J., Brauner, C. J., Wang, Y. X., Richards, J. G., Patrick, M. L., Xi, W., Matey, V., & Val, A. L. (2010). Impact of ontogenetic changes in branchial morphology on gill function in *Arapaima gigas*. *Physiological and Biochemical Zoology*, 83(2), 322– 332.

• Gonzalez, R. J., Wilson, R. W., Wood, C. M., Patrick, M. L., & Val, A. L. (2002). Diverse strategies for ion regulation in fish collected from the ion-poor, acidic Rio Negro. *Physiological and Biochemical Zoology*, 75(1), 37– 47.

• Graham, J. B. (1997). Air-breathing fishes: Evolution, diversity and adaptation. Academic Press.

• Hill, R. W., Armstrong, E. J., Inaba, K., Morita, M., Tresguerres, M., Stillman, J. H., Roa, J. N., & Kwan, G. T. (2018). Acid secretion by the boring organ of the burrowing giant clam, *Tridacna crocea*. *Biology Letters*, 14(6), 20180047.

• Hochachka, P. W., Moon, T. W., Bailey, J., & Hulbert, W. C. (1978). The osteoglossid kidney: Correlations of structure, function, and metabolism with transition to air breathing. *Canadian Journal of Zoology*, 56, 820– 832.

• Howard, V., & Reed, M. (2004). *Unbiased stereology: Three-dimensional measurement in microscopy*. Garland Science.

• Kwan, G. T., Smith, T. R., & Tresguerres, M. (2020). Immunological characterization of two types of ionocytes in the inner ear epithelium of Pacific Chub Mackerel (*Scomber japonicus*). *Journal of Comparative Physiology B*, 190(4), 419– 431.

• Kwan, G. T., Wexler, J. B., Wegner, N. C., & Tresguerres, M. (2019). Ontogenetic changes in cutaneous and branchial ionocytes and morphology in yellowfin tuna (*Thunnus albacares*) larvae. *Journal of Comparative Physiology B*, 189(1), 81– 95.

• Lebovitz, R. M., Takeyasu, K., & Fambrough, D. (1989). Molecular characterization and expression of the ($Na^+ + K^+$)-ATPase alpha-subunit in *Drosophila melanogaster*. *The EMBO Journal*, 8(1), 193– 202.

• Lüling, K. H. (1964). Zur biologie und ökologie von *Arapaima gigas* (pisces, osteoglossidae). *Zeitschrift für Morphologie und Ökologie der Tiere*, 54(4), 436– 530.

• Mühlfeld, C., Nyengaard, J. R., & Mayhew, T. M. (2010). A review of state-of-the-art stereology for better quantitative 3D morphology in cardiac research. *Cardiovascular Pathology*, 19(2), 65– 82.

• Parks, S. K., Tresguerres, M., & Goss, G. G. (2008). Theoretical considerations underlying Na^+ uptake mechanisms in freshwater fishes. *Comparative Biochemistry and Physiology Part C: Toxicology & Pharmacology*, 148(4), 411– 418.

• Pelster, B., & Wood, C. M. (2018). Ionoregulatory and oxidative stress issues associated with the evolution of air-breathing. *Acta Histochemica*, 120(7), 667– 679.

• Pelster, B., Wood, C. M., Braz-Mota, S., & Val, A. L. (2020). Gills and air-breathing organ in O_2 uptake, CO_2 excretion, N-waste excretion, and ionoregulation in small and large pirarucu (*Arapaima gigas*). *Journal of Comparative Physiology B*, 190(5), 569– 583.

• Perry, S. F. (1978). Quantitative anatomy of the lungs of the red-eared turtle, *Pseudemys scripta elegans*. *Respiration Physiology*, 35(3), 245– 262.

• Phuong, L. M., Huong, D. T. T., Malte, H., Nyengaard, J. R., & Bayley, M. (2018). Ontogeny and morphometrics of the gills and swim bladder of air-breathing striped catfish *Pangasianodon hypophthalmus*. *The Journal of Experimental Biology*, 221(3), jeb168658.

• R Core Team. (2018). R: A language and environment for statistical computing. https://www.R-project.org/

• Ramos, C. A., Fernandes, M. N., da Costa, O. T., & Duncan, W. P. (2013). Implications for osmorespiratory compromise by anatomical remodeling in the gills of *Arapaima gigas*. *Anatomical Record (Hoboken)*, 296(10), 1664– 1675.

• Randall, D. J., Farrell, A. P., & Haswell, M. S. (1978). Carbon dioxide excretion in the pirarucu (*Arapaima gigas*), an obligate air-breathing fish. *Canadian Journal of Zoology*, 56, 977– 982.

• Roa, J. N., Munévar, C. L., & Tresguerres, M. (2014). Feeding induces translocation of vacuolar proton ATPase and pendrin to the membrane of leopard shark (*Triakis semifasciata*) mitochondrion-rich gill cells. *Comparative Biochemistry and Physiology Part A: Molecular & Integrative Physiology*, 174, 29– 37.

• Roa, J. N., & Tresguerres, M. (2017). Bicarbonate-sensing soluble adenylyl cyclase is present in the cell cytoplasm and nucleus of multiple shark tissues. *Physiological Reports*, 5(2), e13090.

• Rombough, P. J. (2002). Gills are needed for ionoregulation before they are needed for O_2 uptake in developing zebrafish, *Danio rerio*. *Journal of Experimental Biology*, 205(12), 1787– 1794.

• Rombough, P. J., & Moroz, B. M. (1990). The scaling and potential importance of cutaneous and branchial surfaces in respiratory exchange in young chinook salmon (*Oncorhynchus tshawytscha*). *Journal of Experimental Biology*, 154, 1– 12.

• Rombough, P. J., & Ure, D. (1991). Partitioning of oxygen uptake between cutaneous and brachial surfaces in larval and juvenile chinook salmon *Oncorhynchus tshawytscha*. *Physiological Zoology*, 64(3), 717– 727.

• Sardella, B., & Brauner, C. (2007). Cold temperature-induced osmoregulatory failure: The physiological basis for tilapia winter mortality in the Salton Sea. *California Fish and Game*, 93(4), 200– 213.

• Schindelin, J., Arganda-Carreras, I., Frise, E., Kaynig, V., Longair, M., Pietzsch, T., & Cardona, A. (2012). Fiji: An open-source platform for biological-image analysis. *Nature Methods*, 9(7), 676- 682.

• Shartau, R., & Brauner, C. (2014). Acid–base and ion balance in fishes with bimodal respiration. *Journal of Fish Biology*, 84(3), 682– 704.

• Signorell, A., Aho, K., Alfons, A., Anderegg, N., Aragon, T., Arppe, A., & Borchers, H. (2020). DescTools: Tools for descriptive statistics. R package version 0.99. 34.

• Stevens, E. D., & Holeton, G. F. (1978). The partitioning of oxygen uptake from air and from water by the large obligate air-breathing teleost pirarucu (*Arapaima gigas*). *Canadian Journal of Zoology*, 56, 974–976.

• Tang, C.-H., Leu, M.-Y., Shao, K., Hwang, L.-Y., & Chang, W.-B. (2014). Short-term effects of thermal stress on the responses of branchial protein quality control and osmoregulation in a reef-associated fish *Chromis viridis*. *Zoological Studies*, 53(1), 1– 9.

• Tresguerres, M., Katoh, F., Fenton, H., Jasinska, E., & Goss, G. G. (2005). Regulation of branchial V-H^+-ATPase, Na^+/K^+-ATPase and NHE2 in response to acid and base infusions in the Pacific spiny dogfish (*Squalus acanthias*). *Journal of Experimental Biology*, 208(2), 345– 354.

• Tresguerres, M., Katoh, F., Orr, E., Parks, S. K., & Goss, G. G. (2006). Chloride uptake and base secretion in freshwater fish: A transepithelial ion-transport metabolon? *Physiological and Biochemical Zoology*, 79(6), 981– 996.

• Tresguerres, M., Katz, S., & Rouse, G. W. (2013). How to get into bones: Proton pump and carbonic anhydrase in *Osedax* boneworms. *Proceedings of the Royal Society B: Biological Sciences*, 280(1761), 20130625.

• Val, A. L., & de Almeida-Val, V. M. (1995). Fishes of the Amazon and their environment: Physiological and biochemical features. Springer Verlag.

• Weibel, E. R., & Knight, B. W. (1964). A morphometric study on the thickness of the pulmonary air-blood barrier. *The Journal of Cell Biology*, 21(3), 367– 384.

• Wilson, J., Randall, D. J., Donowitz, M., Vogl, A. W., & Ip, A. K. (2000). Immunolocalization of ion-transport proteins to branchial epithelium mitochondria-rich cells in the mudskipper (*Periophthalmodon schlosseri*). *Journal of Experimental Biology*, 203(15), 2297– 2310.

• Wilson, J., Whiteley, N., & Randall, D. (2002). Ionoregulatory changes in the gill epithelia of coho salmon during seawater acclimation. *Physiological and Biochemical Zoology*, 75(3), 237– 249.

• Wood, C. M., Pelster, B., Braz-Mota, S., & Val, A. L. (2020). Gills versus kidney for ionoregulation in the obligate air-breathing *Arapaima gigas*, a fish with a kidney in its air-breathing organ. *Journal of Experimental Biology*, 223(20), jeb232694.